Asian Journal of Chemistry; Vol. 38, No. 2 (2026), 359-370
ASIAN JOURNAL OF CHEMISTRY
https://doi.org/10.14233/ajchem.2026.34981

Design, Synthesis, Characterization, Molecular Docking, MM/GBSA and Biological Evaluation of Thiazolidinones Derivatives as Promising Antibacterial and Antifungal Agents

SHABNAM THAKUR[1], MOHINI KALRA[1,*], NAVEEN KHATRI[2] and RITU DAHIYA[3]

[1]Amity Institute of Pharmacy, Amity University, Gurugram-121004, India
[2]College of Pharmacy, Swami Dayanand Post Graduate Institute of Pharmaceutical Sciences, Pandit Bhagwat Dayal Sharma University of Health Sciences, Rohtak-124001, India
[3]School of Pharmacy, Lingaya's Vidyapeeth (Deemed to be University), Faridabad-121002, India

*Corresponding author: E-mail: mkalra@ggn.amity.edu

Received: 29 September 2025 *Accepted*: 22 December 2025 *Published online*: 31 January 2026 AJC-22254

In present study, a series of 24 thiazolidinone derivatives (**TH7-TH30**) was rationally designed as potential antibacterial and antifungal agents, of which twelve compounds (**TH7-TH18**) were successfully synthesized and fully characterized using IR, ^{1}H NMR, ^{13}C NMR, and HRMS techniques. The antimicrobial activity of the synthesized derivatives was evaluated by the tube dilution method, and minimum inhibitory concentrations (MICs) were determined against selected bacterial and fungal strains. To elucidate the molecular basis of activity, *in silico* studies were performed on all designed compounds using molecular docking with the Glide module of Schrödinger 9.6. Docking investigations targeted MurB (PDB ID: 7OSQ) and lanosterol 14-α demethylase (PDB ID: 5V5Z), key enzymes involved in bacterial cell wall synthesis and fungal sterol biosynthesis, respectively. Binding modes were further analyzed through superimposition with standard inhibitors, streptomycin for MurB and ketoconazole for lanosterol 14-α demethylase. The stability and binding free energies of the docked complexes were assessed using MM/GBSA calculations. Furthermore, ADMET properties of the designed derivatives were predicted using QikProp (v3.5) to evaluate drug-likeness, oral bioavailability and gut blood barrier permeability. Based on the combined experimental and computational findings, novel thiazolidinone derivatives emerge as promising lead structures for the further development of antibacterial and antifungal agents.

Keywords: Thiazolidinone derivatives, Molecular docking, ADMET analysis, MurB inhibitors, Lanosterol 14-α demethylase.

INTRODUCTION

The rise in the prevalence of antimicrobial resistance (AMR) is a serious global health issue today, undermining the efficacy of current antibacterial and antifungal therapy. Methicillin-resistant *Staphylococcus aureus* (MRSA) and azole-resistant fungal infections, such as *Candida* and *Aspergillus* infections, are a challenging case for the clinical management [1,2]. The resistance of conventional antibiotics and antifungals occur through various mechanisms like genetic mutations, biofilm production and efflux pumps. This has encouraged scientists or researchers to focus on novel dual-target inhibitors with promising antimicrobial activity against bacterial and fungal infections [3,4]. One of the most successful approaches of antibacterial drug discovery is the inhibition of bacterial cell wall biosynthesis. This has been seen in the case of β-lactams and glycopeptides [5]. An ideal target for antibacterial drug discovery is UDP-N-acetylenolpyruvoylglucosamine reductase (MurB). This enzyme plays an important role in peptidoglycan biosynthesis and hence an ideal target for antibacterial drug discovery [6,7]. In a similar manner, lanosterol 14-α demethylase (CYP51) is an important enzyme in the biosynthesis of ergosterol in fungi. By inhibiting this enzyme the loss of membrane integrity takes place and which leads in killing of fungal cells [8,9]. The dual inhibition of UDP-N-acetylenolpyruvoylglucosamine reductase (MurB) and lanosterol 14-α demethylase is an encourging approach for development of antibacterials as well as antifungals [10].

The heterocycles such as thiazolidinones, possess a five-member ring with a sulfur and nitrogen atom. Due to this structural versatility, it possess many biological activities [11]. Therefore, thiazolidinones are well studied for antibacterial activity with interest in inhibiting significant bacterial enzymes such as UDP-N-acetylenolpyruvoylglucosamine reductase

(MurB) [12]. Many researchers have confirmed that thiazolidinone derivatives are capable of binding to the active site of MurB reductase with strong interaction with catalytic residues and inhibiting enzyme activity [13,14]. Molecular docking studies also confirmed that thiazolidinone derivatives form many bonds such as hydrogen bonds, hydrophobic interactions and π-π stacking interactions in the active site of MurB, with improved binding capacity and inhibitory activity [15]. Furthermore, MM/GBSA binding free-energy calculations indicated that thiazolidinones form stable complexes with MurB, supporting their potential role as effective MurB inhibitors in antibacterial drug discovery [16]. The experimental studies have also demonstrated that systematic structural modifications of the thiazolidinone core significantly enhance binding affinity, improve target selectivity and increase metabolic stability, thereby highlighting thiazolidinones as a promising scaffold for the development of novel antibacterial agents [17].

Lanosterol 14-α demethylase (CYP51), a cytochrome P450 dependent enzyme, catalyzes an indispensable step in fungal ergosterol biosynthesis through the demethylation of lanosterol [18]. Ergosterol is critical for fungal membrane structure, fluidity and function; therefore, its depletion results in severe membrane destabilization and ultimately fungal cell death. Targeting CYP51 represents a validated and clinically successful antifungal strategy, forming the molecular basis for azole therapeutics such as ketoconazole and fluconazole [19]. Recent studies have shown that thiazolidinone derivatives are potent CYP51 inhibitors by interacting with the active site of the enzyme, blocking the enzyme from catalyzing the demethylation reaction [20]. Studies show that further structural modifications of the thiazolidinone scaffold can enhance CYP51 selectivity, reducing potential cross-reactivity with human enzymes and enhancing therapeutic efficacy [21]. The present work is aimed to design and evaluate a novel series of thiazolidinone derivatives (**TH7-TH30**) as potential inhibitors of MurB and lanosterol 14-α demethylase using molecular docking, MM/GBSA free energy calculations and ADMET analysis. Molecular docking simulations were conducted using the Glide module of Schrödinger 9.6 and binding stability was assessed using MM/GBSA calculations. Further, *in silico* ADMET profiling using QikProp was performed to assess drug-likeness, oral bioavailability, metabolic stability and CNS penetration potential. This arch works is an attempt at evaluating thiazolidinone derivatives as dual-target inhibitors, providing a framework for the development of new antibacterial and antifungal therapy.

EXPERIMENTAL

All the chemicals used in this study were procured from Aritech Chemazone Pvt Ltd., India. The progress of the reactions was checked by TLC using Merck precoated silica gel G 60 F_{254} plates with 20 × 20 cm dimensions. The developing solvent systems (eluents) consisted of hexane/ethyl acetate mixtures in ratios of 7:3 and 1:1 (v/v). For visualizing the spots of compounds on TLC plates, the plates were located by UV irradiation at 254 nm or exposing to iodine vapours. Melting points were measured by the open capillary method with electric melting point apparatus of icon instruments and are uncorrected.

^{1}H NMR spectra of all the synthesized compounds were recorded on a Bruker Avance NEO 500 MHz spectrometer in $CDCl_3$ solvent using tetramethyl silane as an internal standard. The IR spectra were recorded on an Agilent FTIR (Resolution Pro software). The mass spectra were recorded using Agilent Mass Spectrometry (ESI) with ACQ Optimizer.

General procedure for the synthesis of substituted thiourea derivatives: To synthesize substituted thiourea derivatives, 0.01 mol of a heterocyclic amine, such as 4-aminopiperidine/4-aminopyridine/4-aminoquinazoline (1.00 g), was dissolved in 50 mL of ethanol in a round-bottom flask equipped with a reflux condenser. Subsequently 0.01 mol of substituted isothiocyanate (0.73 g) was added in a 1:1 molar ratio to the solution [22]. The mixture was heated under reflux at approximately 78 ºC with continuous stirring for 6-8 h. The progress of the reaction was monitored with TLC, until the completion of reaction was confirmed. The reaction mixture was cooled to room temperature, inducing precipitation of the substituted thiourea derivative. The precipitate was filtered, washed with cold ethanol to remove residual impurities and dried to afford the pure thiourea derivatives (**Scheme-I**).

General procedure for the synthesis of substituted thiazolidin-4-one derivatives (TH7-TH18): Thiazolidin-4-one derivatives were synthesized *via* a condensation reaction

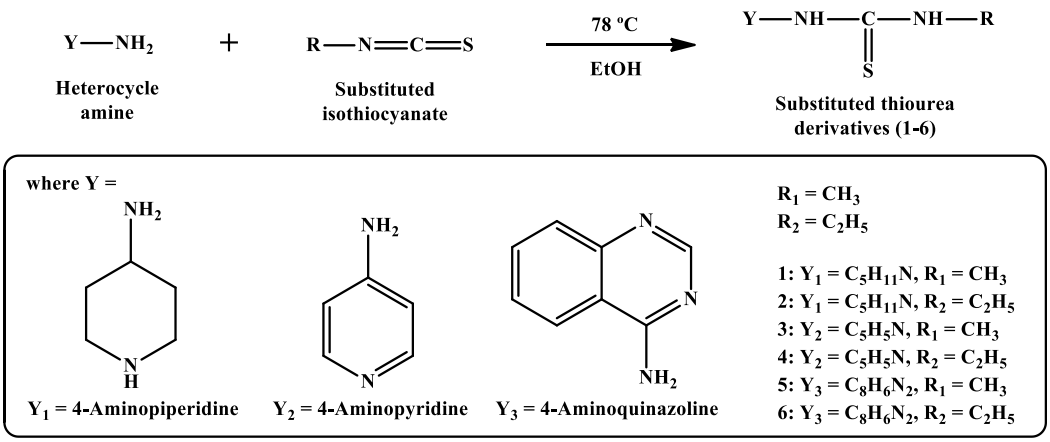

Scheme-I: Synthesis of substituted thiourea derivatives

between substituted thiourea derivatives and acetylenic esters in ethanol. Briefly, substituted thiourea (0.01 mol, 1.74 g) was dissolved in 50 mL of ethanol in a round-bottom flask. To this stirred solution, an equimolar amount of acetylenic ester (0.01 mol, 1.42 g) was added dropwise. The reaction mixture was heated at 50-70 ºC with continuous stirring for 8-10 h to ensure complete cyclization. Reaction progress was monitored by thin-layer chromatography (TLC). The cyclization proceeds *via* nucleophilic attack of the thiourea sulfur atom on the acetylenic ester, leading to the formation of thiazolidin-4-one ring, as illustrated in **Scheme-II**.

Methyl (*Z*)-2-((*Z*)-3-methyl-4-oxo-2-(piperidin-4-ylimino)-thiazolidin-5-ylidene)acetate (TH7): Off-white solid; yield: 54%; m.p.: 140-143 ºC, R_f: 0.60 (hexane/ethyl acetate, 7:3); ^{1}H NMR (500 MHz, $CDCl_3$-d_6) δ 6.88 (1H, s), 3.86 (1H, s), 2.60 (1H, s), 2.59 (1H, s), 2.56 (1H, s), 1.69 (1H, s), 1.58 (1H, s), 1.55 (1H, s). HRMS for $C_{12}H_{17}N_3O_3S$ $[M + H]^+$ *m/z*: calcd. 283.100; observed 284.2300.

Ethyl (Z)-2-((*Z*)-3-methyl-4-oxo-2-(piperidin-4-ylimino)-thiazolidin-5-ylidene)acetate (TH8): Off-greenish solid; yield: 42%; m.p.: 155-157 ºC, R_f: 0.65 (hexane/ethyl acetate, 7:3); IR (KBr, ν_{max}, cm^{-1}): 3432.01 (N–H (amine *str.*) 3088.79 (C–H *str.*, aromatic) 2927.41, 2859.43 (C–H *str.*, aliphatic), 1729.66 (C=O *str.*, ester group), 1646.65 (C=O *str.*, thiazolidine ring), 1628.03 (C=C *str.*, aromatic ring), 1598.06 (C=N *str.*, imine group), 1525.01 and 1473.97 (C–H bending of C-C), 1159.75 (C-N *str.*, thiazolidine ring), 1384.42 (C-O *str.* for ester), 723.46, 707.02 (C–H bending of thiazolidinone ring); ^{1}H NMR (500 MHz, $CDCl_3$-d_6, δ ppm): 6.88 (1H, s), 3.57 (1H, s), 2.91 (1H, s), 2.59 (1H, s), 1.65 (1H, s), 1.54 (1H, s), 1.49 (1H, s), 1.25 (1H, s). HRMS for $C_{13}H_{19}N_3O_3S$ $[M + H]^+$ *m/z*: calcd. 297.112; observed 298.7200.

Methyl (*Z*)-2-((Z)-3-ethyl-4-oxo-2-(piperidin-4-ylimino)-thiazolidin-5-ylidene)acetate (TH9): Red solid; yield: 60%; m.p.: 133-135 ºC, R_f: 0.60 (hexane/ethyl acetate, 7:3); IR (KBr, ν_{max}, cm^{-1}): 3425.10 (N–H amine *str.*) 2960.60 (C–H *str.*, aliphatic), 3099.85 (C–H *str.*, aromatic), 1718.74 (thiazolidinone C=O *str.*), 1645.45 (imine C=N *str.*), 1623.34 (C=C *str.* of alkene), 1233.62 (C-O *str.* (ester) and C-N *str.*), 714.96 (C–S *str.* of thiazolidine); ^{1}H NMR (500 MHz, $CDCl_3$-d_6, δ ppm): 6.88 (s, 1H), 3.90 (s, 1H), 3.67 (s, 1H), 3.60 (s, 1H), 2.28 (s, 1H), 2.24 (s, 1H), 2.22 (s, 1H), 1.93 (s, 1H), 1.89 (s, 1H), 1.81 (s, 1H), 1.26 (s, 1H); HRMS for $C_{13}H_{19}N_3O_3S$ $[M + H]^+$ *m/z*: calcd. 297.110; observed 298.5600.

Ethyl (*Z*)-2-((*Z*)-3-ethyl-4-oxo-2-(piperidin-4-ylimino)-thiazolidin-5-ylidene)acetate (TH10): White solid; yield: 39%; m.p.: 170-173 ºC, R_f: 0.65 (hexane/ethyl acetate, 7:3); IR (KBr, ν_{max}, cm^{-1}): 3420.73 (N–H *str.*, amine *str.*), 3096.11, 3022.75 (C–H *str.*, aromatic), 2966.13, 2857.14 (C–H *str.*, aliphatic), 1726.14 (thiazolidinone C=O *str.*), 1652.14, 1626.84, (C=C *str.*, aromatic), 1513.25 (C=N *str.*, imine), 1175.92, 1116.17, 1040.00, 1015.13 (C-N *str.*, amines/imines), 723.45 (C–S *str.* of thiazolidine); ^{1}H NMR (500 MHz, $CDCl_3$, δ ppm): 6.88-6.23 (2H, m, Ar–H), 5.41-4.89 (2H, m/overlap), 3.47-3.02 (2H, m), 2.59-2.15 (4H, m/overlap), 1.95-1.55 (3H, m), 1.26 (1H, s); HRMS for $C_{14}H_{21}N_3O_3S$ $[M + H]^+$ *m/z*: calcd. 311.400; observed 312.1400.

Methyl (*Z*)-2-((*Z*)-3-methyl-4-oxo-2-(pyridin-4-ylimino)-thiazolidin-5-ylidene)acetate (TH11): Creamish solid; yield: 48%; m.p.: 160-163 ºC, R_f: 0.58 (hexane/ethyl acetate, 1:1); IR (KBr, ν_{max}, cm^{-1}): 3422.38 3420.73 (N–H *str.*, amine *str.*), 3099.74, 3077.89 (C–H *str.*, aromatic), 2927.54, 2843.82, (C–H *str.*, aliphatic), 2445.05, 2158.46 (C≡N or C≡C *str.*, nitrile or alkyne), 1638.61, 1595.18 (C=C *str.*, aromatic), 1541.84, 1514.28, (C=N *str.*, imine), 1412.02, 1362.22, 1340.95 (C–H bend., methyl groups), 749.09, 711.23 (C–S *str.* of thiazolidine); ^{1}H NMR (500 MHz, $CDCl_3$ $CDCl_3$, δ ppm): 8.14-6.52 (4H, m, Ar–H), 3.27 (3H, s, OCH_3/N–CH_3). HRMS for $C_{12}H_{11}N_3O_3S$ $[M + H]^+$ *m/z*: calcd. 277.050; observed 278.0000.

Ethyl (*Z*)-2-((*Z*)-3-methyl-4-oxo-2-(pyridin-4-ylimino)-thiazolidin-5-ylidene)acetate (TH12): Orange solid; yield: 33%; m.p.: 161-163 ºC, R_f: 0.60 (hexane/ethyl acetate, 7:3); IR (KBr, ν_{max}, cm^{-1}): 3422.38 3420.73 (N–H *str.*, amine), 3099.74, 3077.89 (C–H *str.* aromatic), 2927.54, 2843.82, (C–H *str.* aliphatic), 2445.05, 2158.46 (C≡N or C≡C *str.*, nitrile or alkyne), 1638.61, 1595.18 (C=C *str.* aromatic), 1541.84, 1514.28 (C=N *str.* imine), 1412.02, 1362.22, 1340.95 (C–H bending methyl groups), 749.09, 711.23 (C–S *str.*, of thiazolidine); ^{1}H NMR (500 MHz, $CDCl_3$, δ ppm): 8.13-7.26 (5H, m, Ar–H), 6.67 (1H, s, C=CH), 4.89 (2H, q, *J* = 7.2 Hz, -OCH_2, ethyl ester), 3.06 (3H, s, N–CH_3), 1.24 (3H, t, *J* = 7.2 Hz, CH_3, ethyl ester); HRMS for $C_{13}H_{13}N_3O_3S$ $[M + H]^+$ *m/z*: calcd. 291.070; observed 292.3000.

Methyl (*Z*)-2-((*Z*)-3-ethyl-4-oxo-2-(pyridin-4-ylimino)-thiazolidin-5-ylidene)acetate (TH13): Reddish solid; yield: 51%; m.p.: 170-173 ºC, R_f: 0.65 (hexane/ethyl acetate, 7:3); IR (KBr, ν_{max}, cm^{-1}): 3397.44, 3267.94 (N–H *str.*, amine), 3081.03, 3022.04 (C–H *str.*, aromatic), 2816.31 (C–H *str.*, aliphatic),

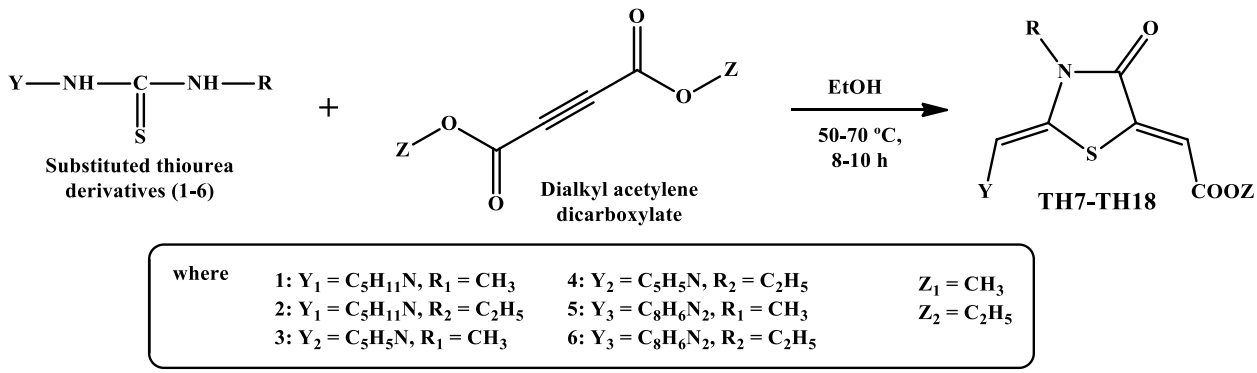

Scheme-II: Synthesis of substituted thiazolidin-4-one derivatives

2320.87 (C=N nitrile), 1695.14 (C=O or carbonyl aromatic ring), 1653.04, 1604.02 (C=C *str.* aromatic ring), 1384.92 (C–H bending methyl groups), 1163.76, (C–N *str.* amines), 1020.19 (C–O *str.*); ^{1}H NMR (500 MHz, $CDCl_3$-d_6, δ ppm): 8.22-7.25 (5H, m, Ar–H), 5.92 (1H, s, C=CH, exocyclic proton), 3.61 (3H, s, -OCH_3, methyl ester), 3.59 (3H, s, N–CH_3), 2.24 (3H, t, *J* = ~7.2 Hz, CH_3, ethyl group). HRMS for $C_{13}H_{13}N_3O_3S$ $[M + H]^+$ *m/z*: calcd. 291.330; observed 292.0000.

Ethyl (*Z*)-2-((*Z*)-3-ethyl-4-oxo-2-(pyridin-4-ylimino)-thia-zolidin-5-ylidene)acetate (TH14): Off white solid; yield: 39%, m.p.: 172–175 ºC, R_f: 0.60 (hexane/ethyl acetate, 7:3); IR (KBr, ν_{max}, cm^{-1}): 3417.96 (O-H or N–H *str.*, broad, hydroxyl or amine/amide), 3082.89, 3025.30, 2925.77 (C–H *str.*, aromatic or aliphatic), 2643.74, 2334.89 (C≡N or C≡C *str.*, nitrile or alkyne), 1718.57, 1617.32 (C=O *str.*, ester, ketone or carboxyl), 1514.53, 1469.58, 1417.60 (C=C *str.*, aromatic or N-O *str.*, nitro group), 1380.33, 1343.63, 1276.24, 1229.78 (C–H bending and C-O *str.*, ether, ester or phenol), 1079.98, 1036.99, 1016.46 (C-O *str.*, alcohol, carboxylic acid or ester), 936.55, 856.14, 831.59 (aromatic ring vibrations); ^{1}H NMR (500 MHz, $CDCl_3$, δ ppm): 8.21 (1H, d, *J* = 5 Hz), 7.89 (1H, d, *J* = 5 Hz), 7.52-7.51 (4H, m), 5.87 (1H, s), 4.01 (2H, q, *J* = 7.2 Hz), 3.89 (3H, s), 1.31 (3H, t, *J* = 7.2 Hz); HRMS for $C_{13}H_{13}N_3O_3S$ $[M + H]^+$ *m/z*: calcd. 305.080; observed 306.0000.

Methyl (*Z*)-2-((*Z*)-3-methyl-4-oxo-2-(quinazolin-4-yl-imino)thiazolidin-5-ylidene)acetate (TH15): Light yellow solid; yield: 59%; m.p.: 180-183 ºC, R_f: 0.58 (hexane/ethyl acetate, 7:3); IR (KBr, ν_{max}, cm^{-1}): 3440.75 (N–H *str.* amine), 3095.05 (C–H *str.* aromatic), 2925.90 (C–H *str.* aliphatic), 2325.35 (C=N *str.* nitrile), 1724.79 (C=O *str.* ester). 1628.03 (C=C *str.* aromatic ring), 1595.36 (C=N *str.* aliphatic), 1340.51 (C–H bending, methyl groups), 1107.70 (C–O *str.* ester); ^{1}H NMR (500 MHz, $CDCl_3$-d_6, δ ppm): 8.18 (6H, m), 7.14 (1H, s), 3.31 (3H, s), 3.19 (3H, s); HRMS for $C_{13}H_{13}N_3O_3S$ $[M + H]^+$ *m/z*: calcd. 328.060; observed 329.2000.

Ethyl (*Z*)-2-((*Z*)-3-methyl-4-oxo-2-(quinazolin-4-yl-imino)thiazolidin-5-ylidene)acetate (TH16): White solid; yield: 62%; m.p.: 185-187 ºC, R_f: 0.62 (hexane/ethyl acetate, 1:1); IR (KBr, ν_{max}, cm^{-1}): 3436.83 (N–H *str.* amine), 3082.33 (C–H *str.* aromatic), 2923.98 (C–H *str.* aliphatic), 2158.92 (C≡C or C≡N *str.*,), 1717.18 (C=O *str.* cyclic ketone), 1617.19 (C=N *str.*, imine), 1566.02, 1515.58 (C=C *str.*, aromatic ring), 1471.78, 1418.16 (C–H bend., CH_2/CH_3), 1381.92, 1343.26 (C–N and/or C–O *str.*), 1277.74, 1241.60, 1205.93 (C–O *str.*, ester), 1168.02 (C–N *str.*, thiazolidinone/ imino), 1080.56, 1035.56, 1015.33 (C–H bending aromatic inplane); ^{1}H NMR (500 MHz, $CDCl_3$, δ ppm): 7.69 (9H, m), 5.97 (1H, s), 4.27 (2H, q, *J* = 7.2 Hz), 3.29 (3H, s), 1.86 (3H, t, *J* = 7.2 Hz). HRMS for $C_{16}H_{14}N_4O_3S$ $[M + H]^+$ *m/z*: calcd. 342.080; observed 342.900.

Methyl (*Z*)-2-((*Z*)-3-ethyl-4-oxo-2-(quinazolin-4-yl-imino)thiazolidin-5-ylidene)acetate (TH17): Creamish solid; yield: 62%; m.p.: 166-169 ºC, R_f: 0.60 (hexane/ethyl acetate, 7:3); IR (KBr, ν_{max}, cm^{-1}): 3434.80 (N–H *str.* amine), 3077.29 (C–H *str.*, aromatic), 2919.06 (C–H *str.*, aliphatic, methyl/ ethyl), 1730.62 (C=O *str.*, ester and lactam/thiazolidinone), 1644.93 (C=N *str.*, imine, quinazolin-4-ylimino), 1596.85 (C=C *str.* aromatic), 1461.89 (CH_3/CH_2 bending), 1378.02 (C–N or C–O bending), 1289.39 (C–O *str.*, ester), 1186.43 (C–N *str.*, thiazolidinone/imino), 1061.69 (C–H inplane bend, aromatic), 992.63 (C–H bending), 861.84 (C–H out-of-plane bend, aromatic/quinazoline); ^{1}H NMR (500 MHz, $CDCl_3$, δ ppm): 7.70 (9H, m), 3.90 (3H, s), 3.90 (2H, q, *J* = 7.2 Hz), 1.58 (3H, t, *J* =7.2 Hz); HRMS for $C_{16}H_{14}N_4O_3S$ $[M + H]^+$ *m/z*: calcd. 342.080; observed 343.1000.

Ethyl (*Z*)-2-((*Z*)-3-ethyl-4-oxo-2-(quinazolin-4-ylimino)-thiazolidin-5-ylidene)acetate (TH18): Brown; yield: m.p.: 175-178 ºC, R_f: 0.60 (hexane/ethyl acetate, 1:1); IR (KBr, ν_{max}, cm^{-1}): 3080 (C–H *str.*, aromatic), 2928, (C–H *str.*, aliphatic, ethyl), 1696 (C=O *str.*, ester and thiazolidinone), 1643–1605 (C=N *str.*, imine, quinazolin-4-ylimino), 1604-1511 (C=C *str.*, aromatic), 1329-1100 (C–N *str.*, thiazolidinone and imino), 1283-1213 (C–O *str.*, ester), 865-824 (C–H out-of-plane bending, aromatic/quinazoline); ^{1}H NMR (500 MHz, $CDCl_3$): δ 7.93 (9H, m), 7.09 (1H, s), 4.27 (2H, q, *J* = 7.2 Hz), 3.29 (3H, s), 1.27 (3H, t, *J* = 7.2 Hz). HRMS for $C_{17}H_{16}N_4O_3S$ $[M + H]^+$ *m/z*: calcd. 356.09; observed 357.000.

Antimicrobial studies: Synthesized thiazolidin-4-one derivatives (**TH7-TH18**) were evaluated for *in vitro* anti-bacterial and antifungal activity using the tube dilution method [23-25]. The compounds were tested against Gram-positive bacteria (*Listeria monocytogenes* ATCC 7644, *Staphylo-coccus aureus* ATCC 33591, *Bacillus subtilis* ATCC 15245), Gram-negative bacteria (*Escherichia coli* ATCC 25922, *Pseudomonas aeruginosa* ATCC 15692) and the yeast *Candida albicans* ATCC 18804. In brief, stock solutions (1000 μg/mL) were prepared and subjected to two-fold serial dilutions in Mueller-Hinton Broth (bacteria) and Sabouraud Dextrose Broth (fungi) to determine the minimum inhibitory concen-trations (MICs). Standardized inocula (0.5 McFarland) were added and the tubes were incubated at 37 ºC for 24 h (bacteria) and 30 ºC for 48 h (*C. albicans*). MICs were recorded as the lowest concentration showing no visible growth. Ciprofloxacin and fluconazole were used as reference standards.

Molecular docking: *In silico* computational simulation was used to rationalize the binding interaction of all the 24 designed thiazolidin-4-one derivatives (**TH7-TH30**) with the target. In order to understand the binding modes of compounds at the molecular level, we carried out the molecular docking simulations of these compounds in the catalytic ligand binding site of the UDP-N-acetylenolpyruvoylglucosamine reductase (MurB) receptor (PDB ID: 7OSQ) and lanosterol 14-α demethy-lase (PDB ID: 5V5Z). The docking was done using Maestro, version 9.6 of the Schrödinger software package.

Ligand & protein preparations: A series of thiazo-lidinone-linked heterocyclic amine derivatives (**TH7-TH30**) was designed using ChemDraw (Fig. 1). Three-dimensional ligand structures were generated in Maestro version 9.6 (Schrödinger) and prepared using the LigPrep module with geometry optimization prior to docking. The crystal structures of MurB (PDB ID: 7OSQ) and lanosterol 14-α demethylase (PDB ID: 5V5Z) were retrieved from the Protein Data Bank [26]. Protein structures were prepared using the Protein Prep-aration Wizard in Maestro, followed by energy minimization, and chain A was selected for docking studies. Receptor grids were generated around the catalytic domains using the Glide module [27], defining the active binding sites for accurate docking. Crystallographic water molecules were removed and

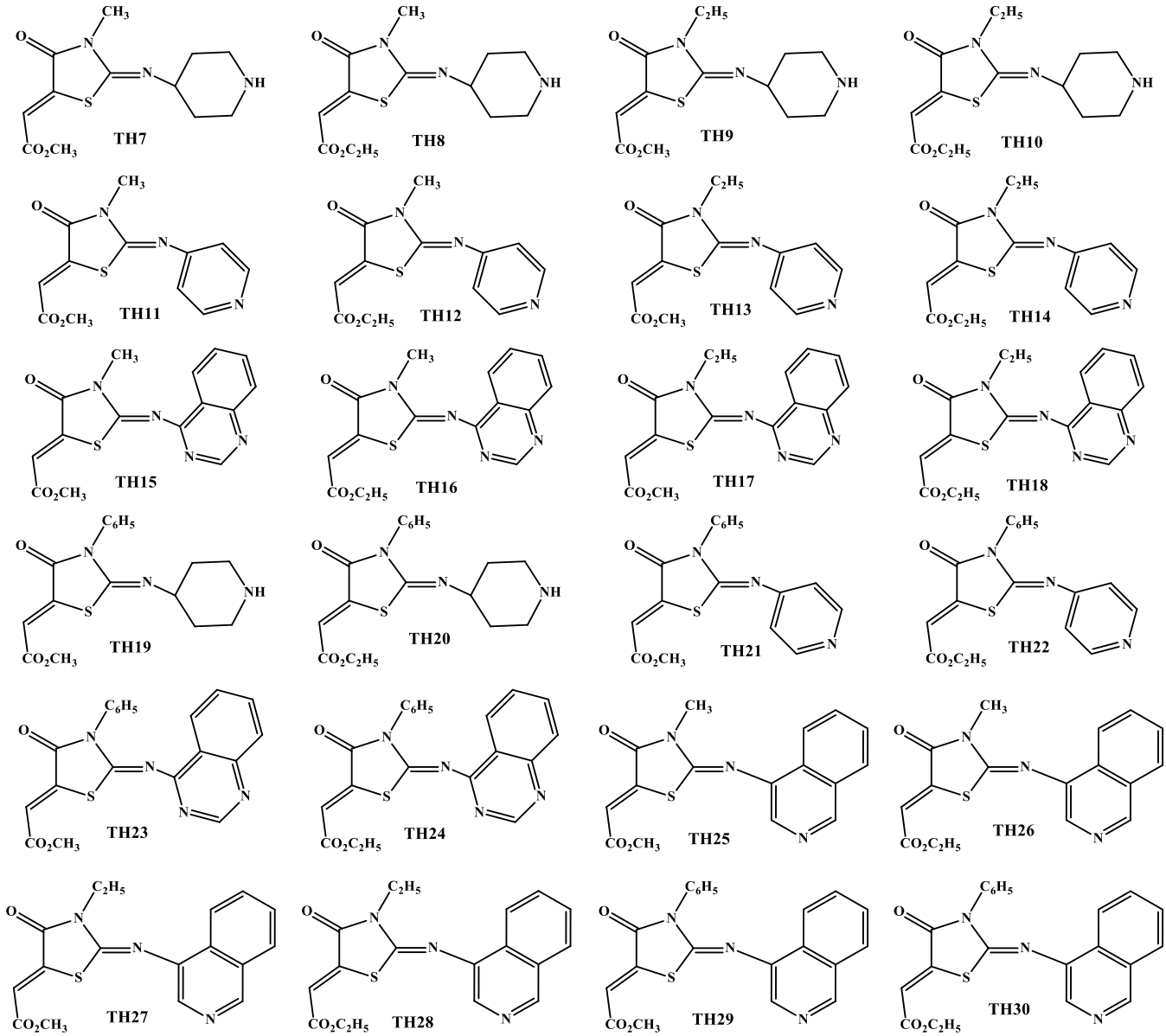

Fig. 1. Structures of designed compounds **TH7-TH30**

van der Waals scaling was applied with a partial charge cutoff of 0.25 [28,29]. Molecular docking of thiazolidin-4-one derivatives (**TH7-TH30**) was performed using Glide extra-precision (XP) mode, retaining up to three top-ranked poses per ligand to evaluate binding interactions with both target enzymes [30].

Molecular mechanics/generalized born surface area (MM/GBSA) analysis: MM-GBSA calculations were performed using the Prime module of Schrödinger v9.6 to estimate the binding free energies (ΔG_{bind}) of selected ligand-receptor complexes [31]. Top-scoring ligand-protein complexes from the docking studies were subjected to MM-GBSA analysis. Energies of the free ligand, receptor and ligand–receptor complexes were calculated following energy minimization using the OPLS3e force field to optimize atomic positions and eliminate steric clashes [32,33]. Calculations were conducted under an implicit solvent model to account for solvation effects and enhance prediction accuracy [34]. The resulting ΔG_{bind} values were used to assess binding stability and interaction strength, enabling identification of the most promising inhibitors of MurB (PDB ID: 7OSQ) and lanosterol 14-α demethylase (PDB ID: 5V5Z) for further evaluation [35].

Absorption, distribution, metabolism, excretion and toxicity (ADMET) analysis: *In silico* ADMET analysis was carried out using the QikProp module of the Schrödinger software suite (v9.6). The designed compounds were assessed for key drug-likeness parameters including molecular weight, polar surface area, central nervous system penetration potential, compliance with Lipinski's rule of five, number of rotatable bonds and the count of nitrogen and oxygen atoms ($^{\#}$N and O). The $^{\#}$stars parameter was employed to identify deviations from established drug-like property ranges.

RESULTS AND DISCUSSION

In this study, a series comprising only 12 thiazolidinone derivatives (**TH7-TH18**) were synthesized and characterized.

The IR spectra of synthesized thiazolidinone of **TH7**-**TH18** reveal a consistent structural framework centered around the thiazolidinone ring, characterized by C=O stretches around 1730-1717 cm^{-1} and C–S stretches around 749-711 cm^{-1}. The presence of amines (N–H *str.* at 3440-3397 cm^{-1}), aromatic rings (C–H stretches at 3099-3077 cm^{-1} and C=C stretches at 1653-1511 cm^{-1}) and imines (C=N stretches at 1650-1513 cm^{-1}) suggests a common scaffold, likely derived from a thiazolidinone core with aromatic and imine substituents. The variations such as nitrile or alkyne stretches in compounds **TH11**, **TH12**, **TH13**, **TH14** and **TH15**, indicate additional functionalization. The presence of ester groups (C-O stretches at 1384-1233 cm^{-1}) in several derivatives suggests esterification, while quinazoline-specific bands in **TH16**, **TH17** and **TH18** point to the incorporation of a quinazoline moiety, a pharmacologically relevant heterocycle.

In ^{1}H NMR, piperidine-containing thiazolidinone derivatives (**TH7**-**TH10**), the methylene protons are differentiated by their proximity to the nitrogen atom. The CH_2 groups located farther from the nitrogen atom resonate as multiplets in the δ 1.40-1.93 ppm range, whereas those adjacent to nitrogen appear downfield at δ 2.24-3.10 ppm due to deshielding induced by the electronegative nitrogen atom. Compounds bearing pyridine moieties (**TH11**-**TH15**) exhibit aromatic or conjugated ring systems and their aromatic protons resonate as doublets, doublets of doublets or complex multiplets between δ 7.26 and 8.22 ppm, reflecting the electron-deficient nature of nitrogen-containing heterocycles.

Alkyl substituents attached to heteroatoms are clearly visible. For example, N-CH_3 groups (**TH7**, **TH8**, **TH11**-**TH16**, **TH18**) appear as singlets in the range of δ 3.06-3.89 ppm, while N-C_2H_5 groups (**TH9**, **TH10**, **TH17**, **TH18**) display characteristic quartet–triplet patterns, with CH_2 signals at δ 3.35-4.27 ppm and CH_3 signals at δ 1.26-1.64 ppm. Ester functionalities are evident in several derivatives (**TH7**-**TH10**, **TH12**-**TH14**, **TH16**, **TH17**), with methyl esters showing singlets at δ 3.61-3.90 ppm and ethyl esters exhibiting quartets (δ 3.57-4.90 ppm) and triplets (δ 1.24-1.86 ppm) corresponding to the ethoxy group. Methoxy (OCH_3) substituents in **TH11**, **TH15** and **TH17** resonate as singlets between δ 3.27 and 3.90 ppm.

Moreover, all compounds (**TH7**-**TH18**) display signals attributable to alkene or exocyclic C=CH protons as singlets in the δ 5.87-7.14 ppm region, indicative of conjugated frameworks such as thiazole or thiazolidinone rings. Derivatives **TH11**-**TH18** further show intense aromatic proton resonances, with pyridine-containing compounds (**TH11**-**TH14**) and bicyclic aromatic systems (**TH15**-**TH18**) exhibiting complex multiplets between δ 7.26 and 8.22 ppm, consistent with extended conjugation and multiple spin-spin interactions.

Antimicrobial assay: Compounds **TH10** and **TH16** exhibited the highest activity against *L. monocytogenes*, each with a minimum inhibitory concentration (MIC) of 3.12 μg/mL, indicating strong antibacterial potential. In contrast, compounds **TH9**, **TH13** and **TH18** were the least active, with MIC values of 25 μg/mL. Against *S. aureus*, compounds **TH8**, **TH15** and **TH17** demonstrated the strongest activity (MIC = 3.12 μg/mL), whereas compound **TH5** showed minimal efficacy (MIC = 25 μg/mL). Owing to their superior performance, com-pounds **TH8**, **TH15** and **TH17** emerged as promising candi-dates for further development (Table-1).

The most potent derivative against *B. subtilis* was compounds **TH12** (MIC = 3.12 μg/mL), while compounds **TH7** and **TH16** displayed the lowest activity (MIC = 25 μg/mL). Despite its relative effectiveness, compound **TH12** was considerably less potent than ciprofloxacin, highlighting the need for structural optimization (Fig. 2). Against *E. coli*, compounds **TH7**, **TH11** and **TH16** showed pronounced antibacterial activity, each with an MIC of 3.12 μg/mL. Conversely, compound **TH10** was the least active (MIC = 25 μg/mL). Although these derivatives performed well within the series, their activity remained inferior to that of the reference drug, indicating

TABLE-1
ANTIMICROBIAL SCREENING (MIC, μg/mL) OF VARIOUS SYNTHESIZED DERIVATIVES

Derivative	Antimicrobial screening (MIC, μg/mL)					
	Antibacterial screening					Antifungal screening
	Listeria monocytogenes ATTC-7644	*Staphylococcus aureus* ATTC-33591	*Bacillus subtilis* ATTC-15245	*Escherichia coli* ATCC-25922	*Pseudomonas aeruginosa* ATCC-15692	*Candida albicans* ATCC-18804
TH7	12.5	6.25	25.0	3.12	6.25	12.5
TH8	6.25	3.12	12.5	6.25	12.5	25.0
TH9	25.0	12.5	6.25	6.25	3.12	6.25
TH10	3.12	6.25	12.5	25.0	6.25	12.5
TH11	12.5	25.0	6.25	3.12	6.25	6.25
TH12	6.25	6.25	3.12	12.5	25.0	12.5
TH13	25.0	12.5	12.5	6.25	3.12	3.12
TH14	12.5	6.25	6.25	12.5	6.25	25.0
TH15	6.25	3.12	6.25	6.25	12.5	3.12
TH16	3.12	12.5	25.0	3.12	6.25	6.25
TH17	12.5	3.12	12.5	6.25	3.12	12.5
TH18	25.0	6.25	6.25	12.5	6.25	6.25
Ciprofloxacin (Ref.)	0.25	0.25	0.25	0.25	0.25	–
Fluconazole (Ref.)	–	–	–	–	–	0.25

scope for further improvement. Compounds **TH9**, **TH13** and **TH17** demonstrated strong activity against *P. aeruginosa* (MIC = 3.12 μg/mL), a significant result given the organism's intrinsic resistance mechanisms. Compound **TH12** was the least effective against this strain (MIC = 25 μg/mL). The observed potency of compounds **TH9**, **TH13** and **TH17** supports their further investigation (Fig. 2).

In antifungal assays, compounds **TH13** and **TH15** showed the highest activity against *C. albicans* (MIC = 3.12 μg/mL), whereas compounds **TH8** and **TH14** were least effective (MIC = 25 μg/mL). Despite their activity, compounds **TH13** and **TH15** were approximately 12.5-fold less potent than fluconazole, underscoring the need for additional optimization prior to clinical consideration (Table-1).

Molecular docking and MM/GBSA analysis for MurB inhibition: The binding affinities of the designed derivatives (**TH7**-**TH30**) toward the MurB receptor (PDB ID: 7OSQ) were evaluated using Glide docking scores and are summarized in Table-2. Among the screened compounds, compound **TH20** exhibited the most favourable docking score, indica-

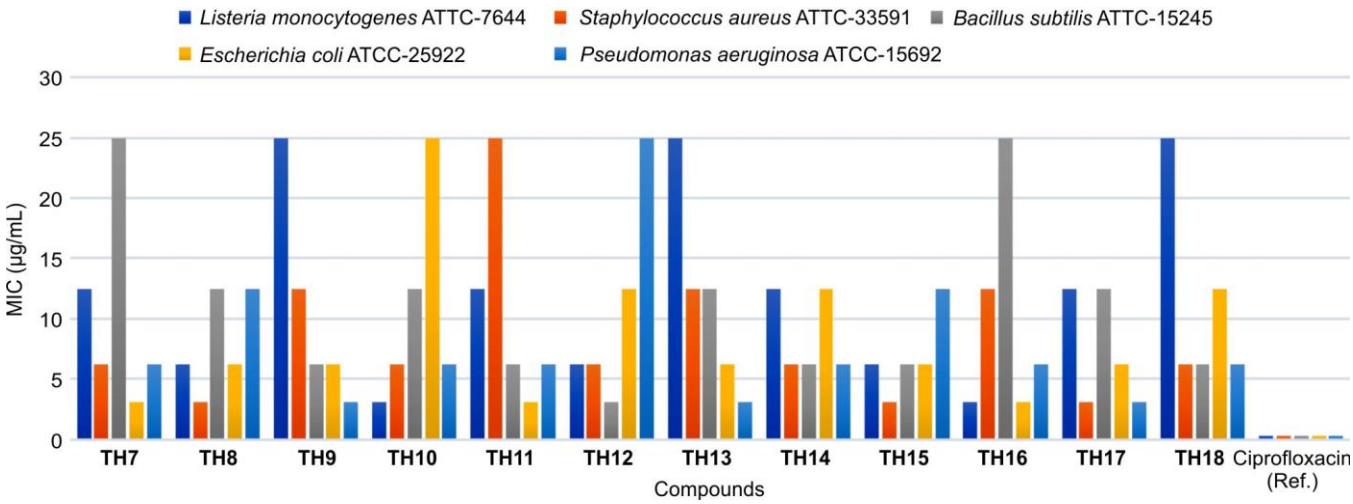

Fig. 2. Antibacterial activity of synthesised **TH7**-**TH18** derivatives

TABLE-2
DOCKING STUDIES FOR COMPOUNDS **TH7**-**TH30** WITH
UDP-N-ACETYLGLUCOSAMINENOLPYRUVATE REDUCTASE (MurB) (PDB ID: 7OSQ)

Compd.	Glide emodel	XP H Bond	Glide gscore	Glide ecoul	XP GScore	Glide Evdw
TH7	-34.233	-0.480	-4.181	-6.494	-4.181	-30.273
TH8	-37.196	-0.700	-4.672	-2.526	-4.672	-25.589
TH9	-38.278	-0.815	-3.669	-2.098	-3.669	-28.208
TH10	-40.912	-0.521	-4.697	-6.608	-4.697	-34.535
TH11	-44.279	-0.869	-4.482	-4.025	-4.482	-29.775
TH12	-42.842	-1.050	-5.438	-4.792	-5.438	-33.061
TH13	-48.099	-0.888	-5.291	-4.879	-5.291	-29.612
TH14	-41.852	-0.700	-4.621	-3.929	-4.621	-29.204
TH15	-47.550	-0.765	-4.430	-3.000	-4.430	-34.970
TH16	-50.049	-0.201	-4.571	-4.520	-4.571	-29.009
TH17	-50.408	-1.014	-4.256	-3.870	-4.256	-35.756
TH18	-54.574	-0.268	-4.450	-2.925	-4.450	-39.106
TH19	-48.637	-0.530	-5.016	-2.699	-5.016	-34.047
TH20	-60.882	-0.389	-5.460	-3.150	-5.460	-39.924
TH21	-46.939	-0.557	-4.341	-3.056	-4.341	-33.398
TH22	-54.153	-0.520	-5.294	-2.065	-5.294	-40.121
TH23	-51.987	-0.913	-5.370	-1.715	-5.370	-35.074
TH24	-56.772	-0.350	-5.391	-1.300	-5.391	-42.034
TH25	-47.421	-0.212	-3.474	-4.520	-3.474	-31.652
TH26	-49.415	-0.177	-4.555	-2.655	-4.555	-33.458
TH27	-46.081	-0.400	-3.633	-1.250	-3.633	-33.199
TH28	-51.173	-0.677	-4.524	-2.078	-4.524	-38.559
TH29	-49.445	-0.798	-5.299	-1.165	-5.299	-35.029
TH30	-55.889	-0.593	-5.367	-2.856	-5.367	-38.064
Streptomyocin (std.)	-58.758	-6.023	-9.893	-17.889	-9.893	-30.355

Glide emodel = glide model energy; XP H Bond = extra precision hydrogen bonding; Glide score = glide score; Glide ecoul = glide Coulomb energy Glide; XP Gscore = extra Precision Glide Score. EvdW = glide vander Waals energy.

ting a strong binding tendency toward the MurB active site. Docking analysis revealed that compound **TH20** formed key hydrogen-bond interactions with Arg166, Tyr132 and Tyr196, residues known to be critical for ligand stabilization within the catalytic domain (Fig. 3). In addition, hydrophobic interactions with Val134, Ile223 and Leu228 further contributed to the stability of the ligand-receptor complex. The LigPlot interaction diagram (Fig. 4) provides a clear representation of these hydrogen-bonding and hydrophobic contacts, illustrating the binding mode of compound **TH20** within the MurB active site.

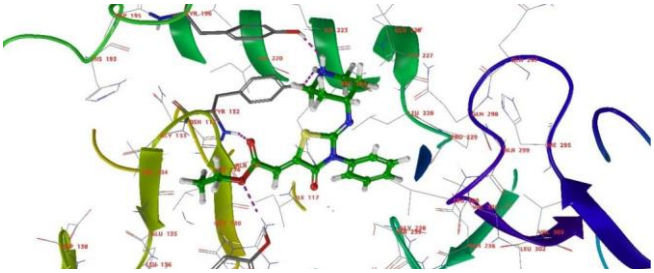

Fig. 3. Binding interaction of highest scoring compound **TH20** (green) against PDB ID: 7OSQ

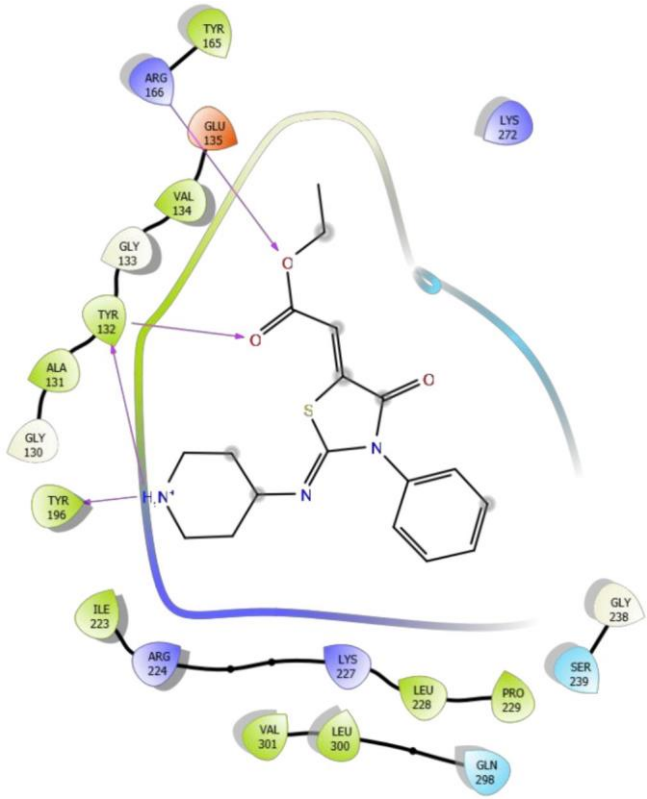

Fig. 4. Ligplot interaction of highest scoring compound **TH20** against PDB ID: 7OSQ

For comparison, the binding interactions of the reference drug streptomycin with MurB were also analyzed. As shown in Fig. 5, streptomycin established multiple hydrogen bonds with essential active-site residues, consistent with its known inhibitory activity. These interactions were further confirmed by the LigPlot analysis (Fig. 6). Superimposition of compound **TH20** and streptomycin within the MurB active site

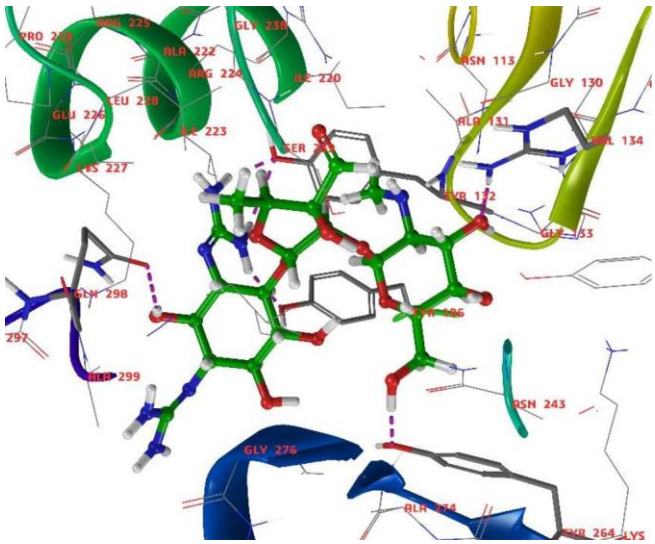

Fig. 5. Binding interaction of standard drug streptomycin (brown) against UDP-N-acetylenolpyruvoylglucosamine reductase (MurB) (PDB ID: 7OSQ)

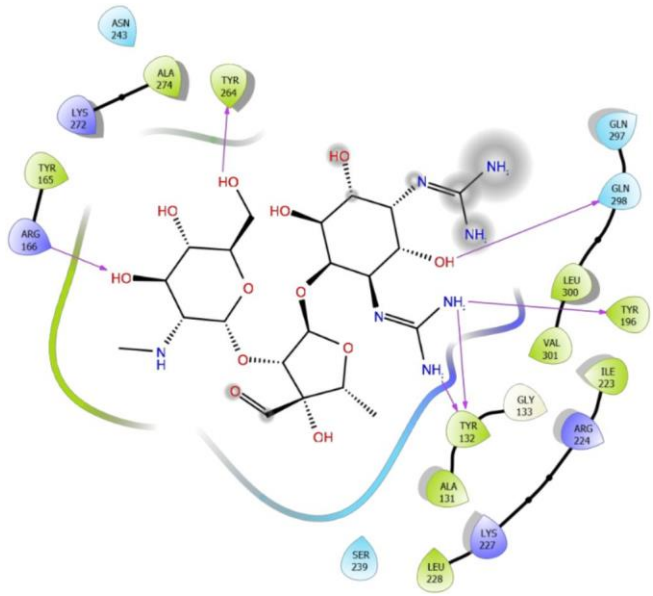

Fig. 6. Ligplot interaction of standard drug streptomycin against PDB ID: 7OSQ

(Fig. 7) demonstrated a comparable binding orientation and interaction pattern, suggesting that compound **TH20** closely mimics the binding behavior of the standard drug. The high degree of structural overlap between compound **TH20** and the MurB binding pocket supports its potential as a novel antimicrobial candidate. Furthermore, comparison of docking scores revealed that compound **TH20** displayed binding affinity comparable to streptomycin, reinforcing its suitability for further development.

The MM/GBSA results revealed a binding free energy of -29.82 kcal mol^{-1} for top-scored compound **TH20**, while streptomycin exhibited a binding free energy of -29.12 kcal mol^{-1}. The minimal difference between these values indicates that compound **TH20** binds to MurB with an affinity comparable to or slightly better than the reference drug. These findings support the strong and stable interaction of compound **TH20**

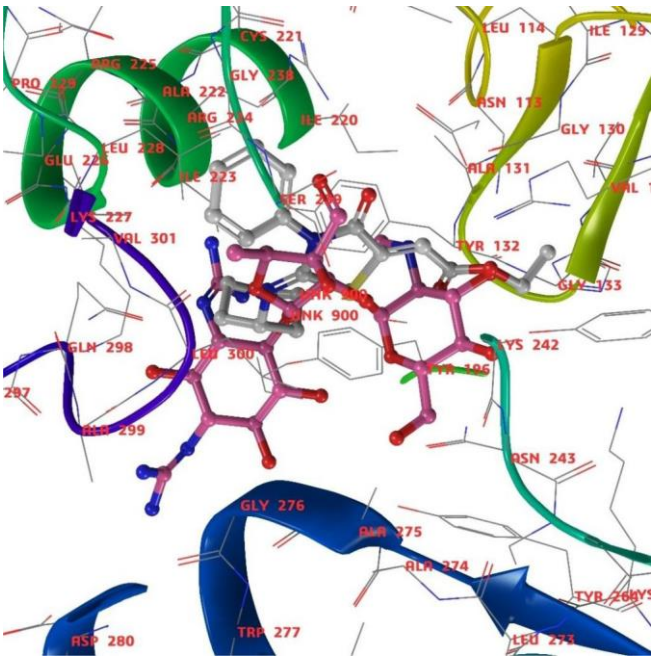

Fig. 7. Superimposition of highest scoring compound (white) with streptomycin (pink) against PDB ID: 7OSQ

within the MurB active site and validate the molecular docking results, highlighting the structural compatibility of **TH20** with the receptor binding pocket (Table-3).

Molecular docking and MM/GBSA analysis for lanosterol 14-α demethylase: The binding affinities of all designed compounds **TH7**-**TH30** toward lanosterol 14-α demethylase (PDB ID: 5V5Z) were evaluated using Glide docking scores, as summarized in Table-4. The docking results indicated that all compounds exhibited appreciable binding affinity toward lanosterol 14-α demethylase. Among them, compound **TH27** emerged as the top-scoring derivative, occupying the active-site cavity effectively and forming hydrogen-bond interactions with Hem601, His377 and Ser378 (Fig. 8). LigPlot analysis further revealed stabilizing hydrogen-bond and hydrophobic interactions contributing to ligand retention within the enzyme pocket (Fig. 9). For comparison, ketoconazole demonstrated a similar interaction profile with the catalytic residues (Figs. 10 and 11). Superimposition analysis of compound **TH27** (cyan) and ketoconazole (green) showed a closely aligned binding orientation and conserved interaction pattern with key active-site residues (Fig. 12). Notably, compound **TH27** and ketoconazole displayed comparable docking scores, suggesting the potential of compound **TH27** as an effective inhibitor of lanosterol 14-α demethylase.

TABLE-3
MM/GBSA BINDING FREE ENERGY VALUES OF HIGHEST SCORING COMPOUND **TH20** AND REFERENCE LIGAND (STREPTOMYCIN) AGAINST UDP-N-ACETYLENOLPYRUVOYLGLUCOSAMINE REDUCTASE (MURB) (PDB ID: 7OSQ)

Name of drug	E_{coul}	G_{bind}
Highest scoring compound **TH20**	28.72	-29.82
Streptomycin	27.30	-29.12

TABLE-4
DOCKING STUDIES FOR COMPOUNDS **TH7-TH30** WITH LANOSTEROL 14-α DEMETHYLASE (PDB ID: 5V5Z)

Compd.	Glide emodel	XP H Bond	Glide gscore	Glide ecoul	XP GScore	Glide evdw
TH7	-51.117	-0.674	-5.462	-4.923	-5.462	-30.516
TH8	-53.366	0.0	-6.024	-4.126	-6.024	-35.505
TH9	-47.298	0.0	-6.52	-4.021	-6.52	-28.433
TH10	-52.476	-0.816	-6.85	-3.932	-6.85	-33.65
TH11	-49.692	-0.168	-5.754	-3.486	-5.754	-29.156
TH12	-50.072	-0.652	-6.487	-4.343	-6.487	-33.518
TH13	-49.994	-0.164	-5.432	-2.786	-5.432	-32.727
TH14	-54.708	0.0	-6.42	-4.554	-6.42	-31.181
TH15	-60.659	-0.679	-6.247	-2.407	-6.247	-44.122
TH16	-58.778	-0.049	-6.77	-2.546	-6.77	-44.358
TH17	-67.799	-0.27	-7.647	-4.788	-7.647	-45.022
TH18	-63.785	-0.482	-5.488	-1.039	-5.488	-41.46
TH19	-45.921	0.0	-6.183	-2.531	-6.183	-39.087
TH20	-54.317	0.0	-6.393	-2.066	-6.393	-37.201
TH21	-63.023	0.0	-5.449	-3.095	-5.449	-42.791
TH22	-55.222	-0.667	-6.827	-4.954	-6.827	-37.828
TH23	-33.811	0.0	-5.481	0.611	-5.481	-27.055
TH24	-42.195	-0.03	-6.409	2.604	-6.409	-40.011
TH25	-61.761	-0.756	-7.805	-5.168	-7.805	-44.781
TH26	-63.958	0.0	-6.531	-3.405	-6.531	-37.042
TH27	-67.963	-0.444	-8.377	-5.047	-8.377	-44.801
TH28	-72.493	-0.583	-7.221	-4.514	-7.221	-45.208
TH29	-40.741	-0.633	-5.139	-0.693	-5.139	-35.662
TH30	-42.624	-0.395	-6.516	0.779	-6.516	-40.121
Ketoconazole	-132.936	-1.505	-8.992	-2.827	-8.992	-66.691

Glide emodel, glide model energy; XP H Bond, extra precision hydrogen bonding; Glide score, glide score; Glide ecoul, glide Coulomb energy Glide; XP Gscore, extra Precision Glide Score. EvdW, glide vander Waals energy.

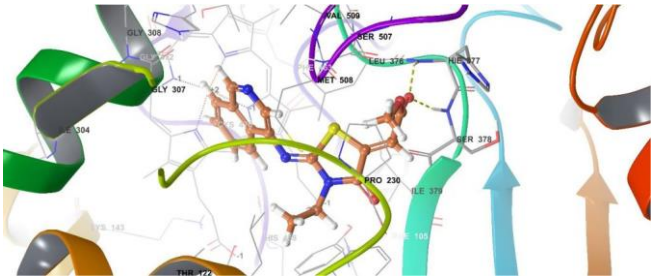

Fig. 8. Binding interaction of highest scoring compound **TH27** (brown) against lanosterol 14-α demethylase (PDB ID: 5V5Z)

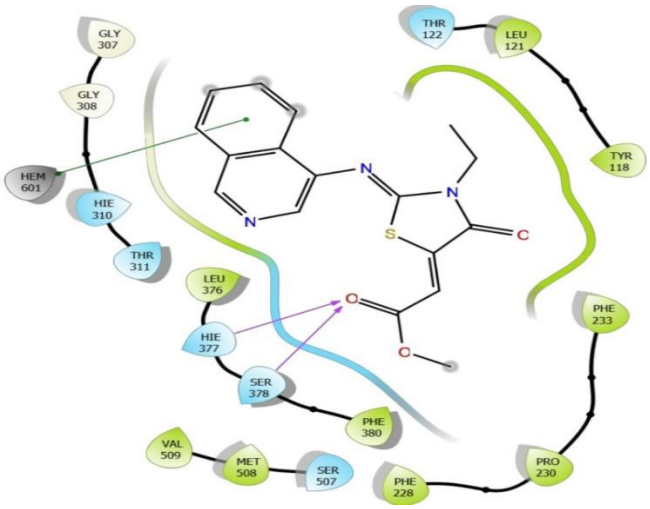

Fig. 9. Ligplot interaction of highest scoring compound **TH27** against lanosterol 14-α demethylase (PDB ID: 5V5Z)

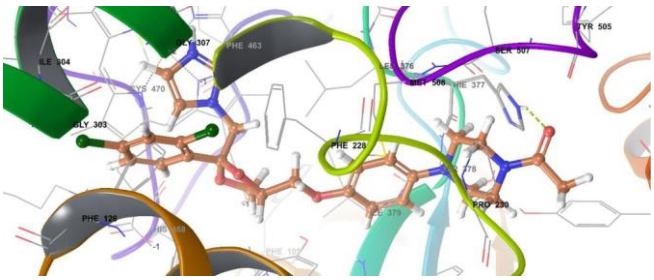

Fig. 10. Binding interaction of standard drug ketoconazole (brown) against lanosterol 14-α demethylase (PDB ID: 5V5Z)

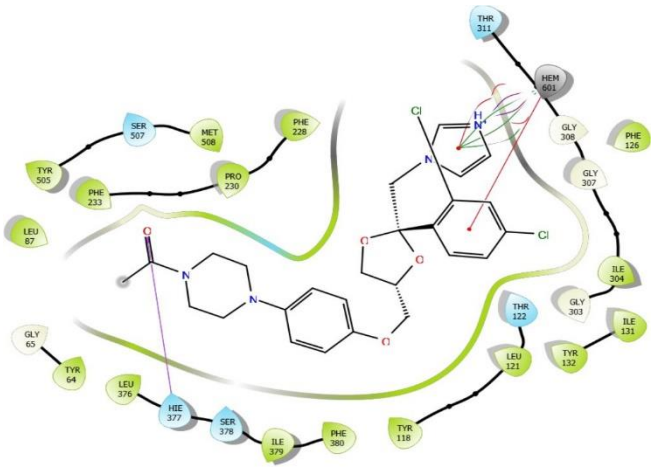

Fig. 11. Ligplot interaction of standard drug ketoconazole against lanosterol 14-α demethylase (PDB ID: 5V5Z)

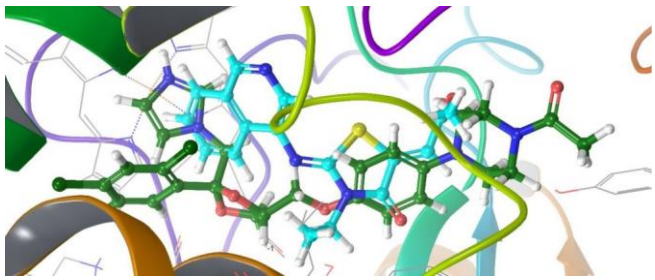

Fig. 12. Superimposition of highest scoring compound **TH27** (cyan) with ketoconazole (green) against lanosterol 14-α demethylase (PDB ID: 5V5Z)

To further assess binding stability, an MM/GBSA analysis was conducted for compound **TH27** within the lanosterol 14-α demethylase active site. The calculated binding free energy for compound **TH27** was -35.83 kcal mol^{-1}, while ketoconazole exhibited a more favourable value of -73.03 kcal mol^{-1} (Table-5). Although compound **TH27** showed lower binding affinity relative to the reference drug, the negative binding free energy indicates a stable ligand-receptor complex. These results validate the docking observations and suggest that compound **TH27** possesses a favourable thermodynamic profile within the enzyme cavity, supporting its potential as a lead candidate for antifungal drug development.

TABLE-5
MM/GBSA BINDING FREE ENERGY VALUES OF HIGHEST SCORING COMPOUND **TH27** AND REFERENCE LIGAND (KETOCONAZOLE) AGAINST LANOSTEROL 14-α DEMETHYLASE (PDB ID: 5V5Z)

Name of drug	E_{coul}	G_{bind}
Highest scoring compound **TH27**	-13.80090867	-35.837538
Ketoconazole	-44.93230198	-73.03473463

ADMET analysis: The predicted QPlog $P_{o/w}$ values, which reflect lipophilicity, ranged from 0.587 to 3.485 for the designed compounds, indicating favourable physico-chemical properties for drug absorption. In contrast, the reference antifungal drug ketoconazole exceeded the recommended range (QPlog $P_{o/w}$ = 4.37), whereas streptomycin exhibited extremely poor lipophilicity (QPlog $P_{o/w}$ = -5.925). All designed derivatives (TH7-TH30) showed zero violations of Lipinski's rule of five, confirming good drug-likeness. By comparison, streptomycin and ketoconazole showed three and one violations, respectively, which may adversely affect their pharmacokinetic behaviour.

Hydrogen-bond donors and acceptors play a critical role in solubility and membrane permeability. All the designed compounds possessed 0-1 hydrogen-bond donors and 7.5-8.0 hydrogen-bond acceptors, supporting efficient passive membrane diffusion. Conversely, streptomycin exhibited a markedly higher number of donors (16) and acceptors (25.25), consistent with its poor permeability across biological membranes.

Predicted human oral absorption (%HOA) values also indicated excellent absorption for most derivatives, ranging from 67.449% to 100%, suggesting high oral bioavailability. Compound **TH20** (QPlog $P_{o/w}$ = 2.111; %HOA = 80.622%) demonstrated an optimal balance of lipophilicity, permeability

and bioavailability, supporting its potential as an antibacterial lead. Similarly, compound **TH27** (QPlog $P_{o/w}$ = 2.085; %HOA = 88.097%) showed favourable pharmacokinetic characteristics consistent with its antifungal potential. Compounds **TH30** (100%), **TH24** (95.268%) and **TH29** (95.154%) exhibited the highest predicted oral absorption. Streptomycin showed 0% predicted oral absorption, confirming its poor gastrointestinal permeability, whereas ketoconazole demonstrated excellent absorption (95.847%).

Overall, the ADMET analysis indicates that the designed compounds possess favourable pharmacokinetic profiles, including suitable lipophilicity, compliance with drug-likeness criteria and high oral absorption. These properties support their potential for further development as inhibitors of MurB and lanosterol 14-α demethylase, as summarized in Table-6.

TABLE-6
In silico ADMET SCREENING FOR PROPOSED COMPOUNDS **TH7-TH30**

Name of drug	QPlogP o/w	Rule of five	Donor HB	Accept HB	% HOA
TH7	0.587	0	1	7.5	67.449
TH8	1.082	0	1	7.5	72.246
TH9	0.937	0	1	7.5	70.42
TH10	1.407	0	1	7.5	74.93
TH11	0.758	0	0	7.5	78.926
TH12	1.017	0	0	7.5	80.164
TH13	1.076	0	0	7.5	82.073
TH14	1.584	0	0	7.5	86.398
TH15	1.371	0	0	8	78.494
TH16	1.488	0	0	8	79.325
TH17	1.518	0	0	8	79.945
TH18	1.959	0	0	8	83.836
TH19	1.989	0	1	7.5	77.559
TH20	2.111	0	1	7.5	80.622
TH21	1.681	0	0	7.5	86.935
TH22	2.638	0	0	7.5	93.31
TH23	2.752	0	0	8	91.238
TH24	3.231	0	0	8	95.268
TH25	1.539	0	0	7.5	80.387
TH26	1.971	0	0	7.5	84.183
TH27	2.085	0	0	7.5	88.097
TH28	2.265	0	0	7.5	86.812
TH29	3.127	0	0	7.5	95.154
TH30	3.485	0	0	7.5	100
Streptomycin	-5.925	3	16	25.25	0
Ketoconazole	4.37	1	0	8.25	95.847

QP logPo/w = predicted octanol/water partition coefficient; Rule of Five = Number of violations of Lipinski's rule of five; Donor HB = estimated number of hydrogen bonds that would be donated by the solute to water molecules in an aqueous solution; Accept HB = Estimated number of hydrogen bonds that would be accepted by the solute from water molecules in an aqueous solution; % HOA = %Human- Oral absorption, Predicted human oral absorption on 0 to 100% scale.

Conclusion

In this study, 24 thiazolidinone derivatives (**TH7-TH30**) were designed with the aim of identifying new antibacterial and antifungal agents. Among these, only 12 derivatives (**TH7-TH18**) were synthesized and structurally characterised using IR, NMR and mass spectrometry techniques. The spectral data confirmed the presence of imine, carbonyl, aromatic and ester moeities, which also contribute to the structural diversity and potential biological relevance. Several thiazolidinone derivatives exhibit significant antibacterial and antifungal activities against Gram-positive (*L. monocytogenes*, *S. aureus*, *B. subtilis*), Gram-negative (*E. coli*, *P. aeruginosa*) and fungal (*C. albicans*) strains, highlighting their therapeutic relevance. The docking studies revealed strong and specific binding of the synthesized compounds within the active sites of MurB and lanosterol 14-α demethylase. Among the series, compound **TH20** exhibited the highest binding affinity toward MurB, underscoring its potential as a lead antibacterial candidate, whereas compound **TH27** showed superior affinity for lanosterol 14-α demethylase, indicating promising antifungal activity. Superimposition analyses further confirmed that the binding orientations of the synthesiszed compounds closely resembled those of the reference inhibitors, streptomycin and ketoconazole, suggesting comparable inhibitory mechanisms. These observations were reinforced by MM/GBSA calculations, which indicated stable ligand-receptor complexes with binding free energies consistent with effective inhibition. ADMET profiling demonstrated that the designed derivatives possess favourable pharmacokinetic characteristics including suitable lipophilicity, high oral absorption and full compliance with Lipinski's rule of five. In particular, compounds **TH20** and **TH27** showed an optimal balance between permeability and bioavailability, supporting their candidacy as drug-like molecules. Furthermore, compounds **TH30**, **TH24** and **TH29** exhibited the highest predicted oral absorption, identifying them as promising scaffolds for further optimization. Overall, compounds **TH20** and **TH27** emerged as the most compelling antibacterial and antifungal lead compounds, respectively. The combined experimental and computational findings indicate that these molecules represent valuable starting points for further structural refinement. Future *in vitro* and *in vivo* studies will be essential to confirm their efficacy, safety and therapeutic potential as MurB and lanosterol 14-α demethylase inhibitors.

CONFLICT OF INTEREST

The authors declare that there is no conflict of interests regarding the publication of this article.

DECLARATION OF AI-ASSISTED TECHNOLOGIES

During the preparation of this manuscript, the authors used an AI-assisted tool(s) to improve the language. The authors reviewed and edited the content and take full responsibility for the published work.

REFERENCES

1. X. Cui, L. Wang, Y. Lü, and C. Yue, *J. Infect. Public Health*, **15**, 986 (2022); https://doi.org/10.1016/j.jiph.2022.08.004
2. J.F. Borgio, A.S. Rasdan, B. Sonbol, G. Alhamid, N.B. Almandil and S. Abdul-Azeez, *Biology*, **10**, 1144 (2021); https://doi.org/10.3390/biology10111144
3. J.M. Blair, M.A. Webber, A.J. Baylay, D.O. Ogbolu and L.J. Piddock, *Nat. Rev. Microbiol.*, **13**, 42 (2015); https://doi.org/10.1038/nrmicro3380

4. M. Sanguinetti, B. Posteraro and C. Lass-Flörl, *Mycoses*, **58**, 2 (2015); https://doi.org/10.1111/myc.12330
5. K. Bush, P. Courvalin, G. Dantas, J. Davies, B. Eisenstein, P. Huovinen, G.A. Jacoby, R. Kishony, B.N. Kreiswirth, E. Kutter, S.A. Lerner, S. Levy, K. Lewis, O. Lomovskaya, J.H. Miller, S. Mobashery, L.J.V. Piddock, S. Projan, C.M. Thomas, A. Tomasz, P.M. Tulkens, T.R. Walsh, J.D. Watson, J. Witkowski, W. Witte, G. Wright, P. Yeh and H.I. Zgurskaya, *Nat. Rev. Microbiol.*, **9**, 894 (2011); https://doi.org/10.1038/nrmicro2693
6. J.L. Marquardt, D.A. Siegele, R. Kolter and C.T. Walsh, *J. Bacteriol.*, **174**, 5748 (1992); https://doi.org/10.1128/jb.174.17.5748-5752.1992
7. L.L. Silver, *Clin. Microbiol. Rev.*, **24**, 71 (2011); https://doi.org/10.1128/CMR.00030-10
8. A.G. Warrilow, J.E. Parker, C.L. Price, W.D. Nes, S.L. Kelly and D.E. Kelly, *Antimicrob. Agents Chemother.*, **59**, 7771 (2015); https://doi.org/10.1128/AAC.01806-15
9. D. Sanglard, *Curr. Opin. Microbiol.*, **5**, 379 (2002); https://doi.org/10.1016/S1369-5274(02)00344-2
10. N.P. Wiederhold, *Infect. Drug Resist.*, **10**, 249 (2017); https://doi.org/10.2147/IDR.S124918
11. A. Verma and S.K. Saraf, *Eur. J. Med. Chem.*, **43**, 897 (2008); https://doi.org/10.1016/j.ejmech.2007.07.017
12. C.J. Andres, J.J. Bronson, S.V. D'Andrea, M.S. Deshpande, P.J. Falk, K.A. Grant-Young, W.E. Harte, H.-T. Ho, P.F. Misco, J.G. Robertson, D. Stock, Y. Sun and A.W. Walsh, *Bioorg. Med. Chem. Lett.*, **10**, 715 (2000); https://doi.org/10.1016/S0960-894X(00)00073-1
13. J. Heijenoort, *Nat. Prod. Rep.*, **18**, 503 (2001); https://doi.org/10.1039/a804532a
14. S. Ahmed, M.F. Zayed, S.M. El-Messery, M.H. Al-Agamy and H.M. Abdel-Rahman, *Molecules*, **21**, 568 (2016); https://doi.org/10.3390/molecules21050568
15. C. Tratrat, A. Petrou, A. Geronikaki, M. Ivanov, M. Kostić, M. Soković, I.S. Vizirianakis, N.F. Theodoroula and M. Haroun, *Molecules*, **27**, 1930 (2022); https://doi.org/10.3390/molecules27061930
16. K. Omar, A. Geronikaki, P. Zoumpoulakis, C. Camoutsis, M. Soković, A. Ćirić and J. Glamočlija, *Bioorg. Med. Chem.*, **18**, 426 (2010); https://doi.org/10.1016/j.bmc.2009.10.041
17. D.S. Perlin, R. Rautemaa-Richardson and A. Alastruey-Izquierdo, *Lancet Infect. Dis.*, **17**, e383 (2017); https://doi.org/10.1016/S1473-3099(17)30316-X
18. J. Berman and P.E. Sudbery, *Nat. Rev. Genet.*, **3**, 918 (2002); https://doi.org/10.1038/nrg948
19. J.A. Maertens, *Clin. Microbiol. Infect.*, **10(Suppl. 1)**, 1 (2004); https://doi.org/10.1111/j.1470-9465.2004.00841.x
20. M. Fesatidou, P. Zagaliotis, C. Camoutsis, A. Petrou, P. Eleftheriou, C. Tratrat, M. Haroun, A. Geronikaki, A. Ćirić and M. Soković, *Bioorg. Med. Chem.*, **26**, 4664 (2018); https://doi.org/10.1016/j.bmc.2018.08.004
21. L.M. Podust, J.P. von Kries, A.N. Eddine, Y. Kim, L.V. Yermalitskaya, R. Kuehne, H. Ouellet, T. Warrier, M. Alteköster, J. Rademann, J.S. Lee, H. Oschkinat, S.H.E. Kaufmann and M.R. Waterman, *Antimicrob. Agents Chemother.*, **51**, 3915 (2007); https://doi.org/10.1128/AAC.00311-07
22. A. Doregiraee, E. Tavakolinejad Kermani, H. Khabazzadeh and B. Pouramiri, *J. Chil. Chem. Soc.*, **60**, 3021 (2015); https://doi.org/10.4067/S0717-97072015000300009
23. C.G. Carvalhaes, A.L. Klauer, P.R. Rhomberg, M.A. Pfaller and M. Castanheira, *J. Clin. Microbiol.*, **60**, e02449 (2022); https://doi.org/10.1128/jcm.02449-21
24. J.M. Andrews, *J. Antimicrob. Chemother.*, **48(suppl_1)**, 5 (2001); https://doi.org/10.1093/jac/48.suppl_1.5
25. J. McFarland, *JAMA*, **49**, 1176 (1907); https://doi.org/10.1001/jama.1907.25320140022001f
26. H.M. Berman, J. Westbrook, Z. Feng, G. Gilliland, T.N. Bhat, H. Weissig, I.N. Shindyalov and P.E. Bourne, *Nucleic Acids Res.*, **28**, 235 (2000); https://doi.org/10.1093/nar/28.1.235
27. M.P. Jacobson, R.A. Friesner, Z. Xiang and B. Honig, *J. Mol. Biol.*, **320**, 597 (2002); https://doi.org/10.1016/S0022-2836(02)00470-9
28. T.A. Halgren, R.B. Murphy, R.A. Friesner, H.S. Beard, L.L. Frye, W.T. Pollard and J.L. Banks, *J. Med. Chem.*, **47**, 1750 (2004); https://doi.org/10.1021/jm030644s
29. M. Aarthy, U. Panwar and S.K. Singh, *Sci. Rep.*, **10**, 8661 (2020); https://doi.org/10.1038/s41598-020-65446-7
30. W. Sherman, T. Day, M.P. Jacobson, R.A. Friesner and R. Farid, *J. Med. Chem.*, **49**, 534 (2006); https://doi.org/10.1021/jm050540c
31. P.A. Greenidge, C. Kramer, J.-C. Mozziconacci and R.M. Wolf, *J. Chem. Inf. Model.*, **53**, 201 (2013); https://doi.org/10.1021/ci300425v
32. S. Genheden and U. Ryde, *Expert Opin. Drug Discov.*, **10**, 449 (2015); https://doi.org/10.1517/17460441.2015.1032936
33. D. Shivakumar, J. Williams, Y. Wu, W. Damm, J. Shelley and W. Sherman, *J. Chem. Theory Comput.*, **6**, 1509 (2010); https://doi.org/10.1021/ct900587b
34. N. Homeyer and H. Gohlke, *Mol. Inform.*, **31**, 114 (2012); https://doi.org/10.1002/minf.201100135
35. P.D. Lyne, M.L. Lamb and J.C. Saeh, *J. Med. Chem.*, **49**, 4805 (2006); https://doi.org/10.1021/jm060522a